PAPER Nr.: 4

REVIEW AND ANALYSIS OF THE DNW/MODEL 360 ROTOR ACOUSTIC DATA BASE

BY

R. A. ZINNER AND D. A. BOXWELL
U.S. ARMY AEROFLIGHTDYNAMICS DIRECTORATE, AVSCOM
NASA AMES RESEARCH CENTER
MOFFETT FIELD, CALIFORNIA

R. H. SPENCER
BOEING HELICOPTERS
PHILADELPHIA, PENNSYLVANIA

FIFTEENTH EUROPEAN ROTORCRAFT FORUM

SEPTEMBER 12 - 15, 1989 AMSTERDAM

REVIEW AND ANALYSIS OF THE DNW/MODEL 360 ROTOR ACOUSTIC DATA BASE

R.A. Zinner and D.A. Boxwell

U.S. Army Aeroflightdynamics Directorate, AVSCOM
NASA Ames Research Center
Moffett Field, California 94035 USA

R.H. Spencer

Boeing Helicopters
Philadelphia, Pennsylvania USA

ABSTRACT

A comprehensive model rotor aeroacoustic data base was collected in a large anechoic wind tunnel in 1986. Twenty-six microphones were positioned around the azimuth to collect acoustic data for approximately 150 different test conditions. A dynamically scaled, blade-pressure-instrumented model of the forward rotor of the BH 360 helicopter simultaneously provided blade pressures for correlation with the acoustic data. High-speed impulsive noise, blade-vortex interaction noise, low-frequency noise, and broadband noise were all captured in this extensive data base. This paper presents trends in each noise source, with important parametric variations. The purpose of this paper is to introduce this data base and illustrate its potential for predictive code validation.

SYMBOLS AND ABBREVIATIONS

AATMR	Aerodynamic and Acoustic Testing of Model Rotors
dB	decibels, ref. 0.00002 Pa
B&K	Brüel & Kjær
BBN	broadband noise
BH	Boeing Helicopters (formerly Boeing Vertol)
BPF	blade passage frequency
BVI	blade-vortex interaction
BVWT	Boeing V/STOL Wind Tunnel
BWI	blade-wake interaction
C_T	thrust coefficient in wind axis, $L/\pi\rho\Omega^2R^4$
D	rotor diameter, 121.24 in.
DNW	Duits-Nederlandse Windtunnel
FFT	fast Fourier transform
HSI	high-speed impulsive
ICAO	International Civil Aviation Organization
L	rotor lift, lb
M_{AT}	advancing tip Mach number
M_H	hover tip Mach number

$M_{H_{NOM}}$	nominal hover tip Mach number, 0.636
NLR	Nationaal Lucht-En Ruimtevaartlaboratorium
OLS	Operational Loads Survey
PTP	peak-to-peak
R	rotor radius, 60.62 in.
RPM	revolutions per minute
RWTS	rotary-wing test stand
SPL	sound pressure level
T	rotor thrust, lb
V	velocity
α_s	shaft angle, deg, (+) tilt backward
μ	advance ratio, $V/\Omega R$
Ω	rotational speed, rad/sec
ψ	azimuthal angle, deg, zero over tail, (+) counterclockwise viewed from above
ρ	air density, lb/ft^3
σ	thrust-weighted solidity, 0.10053

1. INTRODUCTION

Helicopter noise was recognized as a problem as early as 1954 when Hubbard and Lassiter wrote their paper entitled "Some Aspects of the Helicopter Noise Problem."[1] Although Hubbard and Lassiter were primarily describing engine and transmission noise, external noise is of even greater concern with today's helicopters. Helicopter noise was officially addressed in 1979 when the International Civil Aviation Organization (ICAO) Committee on Aircraft Noise established limits on the amount of external noise a helicopter could produce under different flight conditions. This new set of standards required manufacturers to produce helicopters that reduced noise below the levels established by the ICAO.[2]

One way to ensure that new helicopters produce noise below the ICAO limits is to use accurate acoustic prediction codes in the early design stages. The confidence level of these prediction codes needs to be high to keep the acoustician an integral part of the design team. One of the most important steps in code development is code validation, for which a high-quality rotor acoustic data base is essential. Unfortunately, only limited high-quality acoustic data have been available for use in validation, often consisting of merely a single point or a single flight condition. This dearth of acoustic data is one of the factors limiting the rapid progress of acoustic prediction codes.

A new rotor acoustic data base is now available to the aeroacoustic research community in a 25-volume, 11-report set.[3] This data base, inspired by a joint agreement between the U.S. Army Aeroflightdynamics Directorate and Boeing Helicopters (BH), was collected in the Duits-Nederlandse Windtunnel (DNW) in 1986. This experimental test was one in a series of tests under the Army's Aerodynamic and Acoustic Testing of Model Rotors (AATMR) program and used a dynamically scaled, blade-pressure-instrumented model of the forward rotor on the BH 360 helicopter.

This paper collates and summarizes the validated acoustic data base in an order that gives careful attention to four areas of current rotor acoustic research: 1) high-speed impulsive (HSI) noise, 2) blade-vortex interaction (BVI) noise, 3) low-frequency noise, and 4) broadband noise (BBN). Each of these basic rotor-noise sources was identified in validat-

ing the BH 360 data base, and the data for each are presented and arranged in terms of trends using critical scaling parameters. These scaling parameters are the same as those already reported in the literature.[4,5] Also to be discussed is the extent to which distinct features of each source exist in this data base, including some known anomalies and deficiencies of which users should be aware when including this data base in specific areas of their rotor acoustic predictive work.

2. DESCRIPTION

Wind Tunnel

The DNW facility is located in the northeastern region of The Netherlands. It is an atmospheric, closed-circuit, subsonic wind tunnel with three interchangeable closed test sections and an open-jet configuration. In the open-jet configuration the walls, ceiling, and floor are anechoically treated (80-Hz cutoff frequency) and have an interior volume greater than 30,000 m^3. This makes the DNW the largest aeroacoustic testing facility in the free world. The maximum obtainable velocity in the open-jet section is 85 m/sec. When velocities greater than 85 m/sec are necessary, one of the three nonanechoic, closed test sections is utilized. A more complete description of the DNW and its capabilities for aeroacoustic testing appears in the literature.[6,7]

Model Rotor

The rotor tested is a 1/5th geometrically and dynamically scaled pressure-instrumented model of the forward rotor of the BH 360 (figure 1). Rotor radius (R) is 60.62 in., with a linear planform taper starting at 90% R. Thickness also tapers from a VR12 cross section to a VR15 cross section starting at 85% R. The blade has a piecewise linear twist distribution with a total twist of -9.3° and is constructed of a composite graphite-Kevlar-epoxy material. Thrust-weighted solidity (σ) is 0.10053. For a more complete description of the rotor[8] see table I.

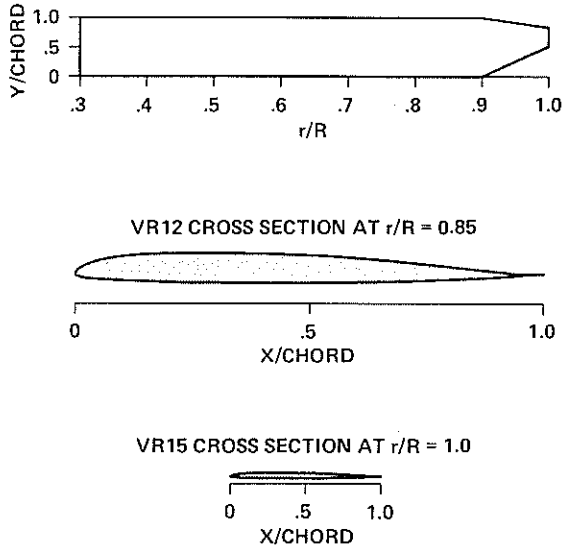

Figure 1. Model BH 360 rotor blade geometry.

Table I. Main Rotor Parameters.

Basic chord, in.	5.285
Radius, in.	60.619
Number of blades, b	4
Taper ratio (tip chord/basic chord)	0.3206
Location of taper start, r/R	0.9
Root cutout, r/R	0.268
Thrust-weighted solidity, σ	0.10053
Airfoil section (0.268R-0.085R)	VR12
Airfoil section (tip)	VR15
Nominal RPM	1323
Nominal hover tip Mach number	0.636
1st flap frequency, Hz	2.626
2nd flap frequency, Hz	4.679
1st chord frequency, Hz	7.8
1st torsion frequency, Hz	5.25

Test Stand

The Aeroflightdynamics Directorate rotary-wing test stand (RWTS) was covered by an acoustically treated housing and affixed to the DNW sting with the rotor at the centerline of the tunnel (figure 2a). This sting was preprogrammed to vertically maintain the rotor hub on the centerline of the tunnel when the shaft-tilt was varied.

The stand is composed of a motor housing, a transmission, an extension shaft, a six-component strain-gauge balance, and a remotely controlled swashplate. Thrust, torque, sideloads, and pitching and rolling moments were measured by the balance. Two Able 60-hp motors powered the model.

Microphone Locations

A specially designed and acoustically treated movable microphone stand held 13 in-flow microphones. This stand moved parallel to the wind axis to keep microphones 1-13 at a constant 1.5-rotor-diameter distance from the hub (figures 2b, c, d). Microphones 14-17 were also in the flow, at a distance of 3.0 rotor diameters directly upstream of the rotor. Microphones 18 and 19 were placed on either side of the RWTS just below the rotor plane for direct comparison with BVWT test 313 data. Microphone 20 was located on-axis directly above the hub at 2.5 rotor diameters, and microphones 21-26 were used for out-of-flow, far-field measurements.

Microphone Type and Calibration

Microphones 1-20 were B&K 1/4-in. (type 4135) and microphones 21-26 were B&K 1/8-in. (type 4185). Each microphone was calibrated using a B&K pistonphone at the beginning or end of each magnetic tape. For intermediate calibrations an insertion voltage-type calibration was performed.

Data-Acquisition Equipment

All data were FM tape recorded on-line and later digitized by a high-speed data-acquisition system. This system consisted of 32 Pacific model 60A integrated amplifier/filters, 32 Preston GMSH sample and hold amplifiers, a Preston GMAD-1 analog-to-digital converter, and a VAX-11/751. A rotor-generated 1024/rev clock was used so that 1024 points per revolution were acquired for each channel for a period of 64 revolutions. All data were analog low-pass-filtered (6-pole Bessel) to 10 kHz prior to digitizing.

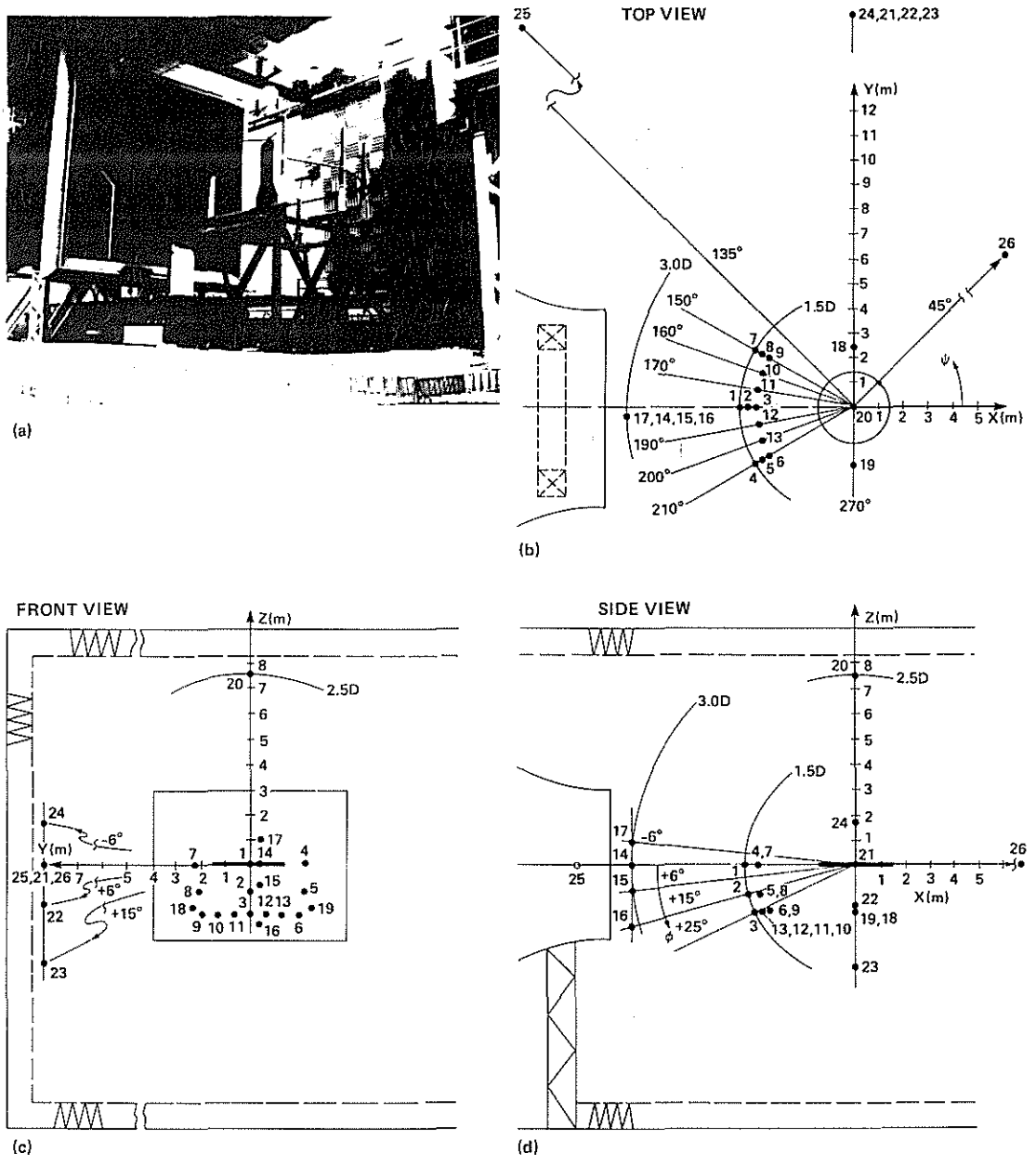

Figure 2. Experimental setup and microphone locations: (a) open jet section, (b) top view, (c) front view, (d) side view.

Test Conditions

Test conditions were chosen to obtain a representative range of rotor-noise conditions. These included high advance ratios ($\mu = 0.329$) combined with high hover tip Mach numbers ($M_H = 0.688$) for HSI noise; hover tip Mach number and thrust sweeps ($M_H = 0.500$ to 0.694 and $C_T/\sigma = 0.002$ to 0.109) for low-frequency noise; and large parametric sweeps of shaft-tilt angle and advance ratio for BVI noise. A complete listing of the test matrix is shown in table II.

Table II. Test matrix.

Condition	C_T/σ	M_H	α_s	μ
M_H sweep	0.069	0.500 to 0.664	0.0	0.00
			-1.2	0.10
		0.501 to 0.694	4.0	0.15
				0.20
M_H sweep	0.069	0.636	-4.6	0.331
			-5.6	0.357
			-4.8	0.342
			-4.5	0.328
α_s sweep	0.069	0.636	0 to 8	0.125
				0.135
				0.150
				0.175
				0.198
				0.225
				0.250
α_s sweep	0.054	0.636	4 to 8	0.150
			2 to 6	0.200
α_s sweep	0.100	0.636	2 to 8	0.150
			2 to 6	0.200
C_T/σ sweep	0.000 to 0.109	0.636	0.0	0.0

3. RESULTS

Data Reduction and Processing

All the data presented in this paper were taken from AATMR reports TR88-1 through TR88-10.[3] The data are available in hardcopy and on digital magnetic tape in four formats: format 1) instantaneous time history; format 2) average of 64 power spectrums; format 3) average of 64 time histories; and format 4) power spectrum of the 64 averaged time histories.

For the HSI-noise time histories presented in this paper, format 3 was used with an additional averaging of each blade's peak negative pressure, to account for blade-to-blade differences. For the HSI-noise frequency data, format 4 was used.

Digital filtering techniques were utilized for all of the BVI-noise data presented, in an attempt to capture the true amplitude of the BVI noise without the influence of thickness noise. The digital filtering process was as follows: A fast Fourier transform (FFT) was performed on the format 3 data, a cutoff frequency was selected, and an inverse FFT was performed to transfer the data back into time histories. Figure 3 is an example of a run with a large amount of BVI, unfiltered and then high-pass-filtered above 220 Hz (220 Hz to 10 kHz). The extraction of the fundamental and first harmonic (0 Hz to 220 Hz) from the spectrum eliminates most of the thickness noise. This 220-Hz cutoff frequency was selected to exclude the minimum number of harmonics necessary to reduce the amplitude of the thickness noise below the smallest of the BVI peak negative pressures. The difference in magnitude between the filtered peak maximum pressure and an adjacent peak minimum pressure (peak-to-peak (PTP) pressure) for each of the four blades was then averaged. These filtered, PTP, 64-revolution-averaged, blade-to-blade averaged data are presented in all of the BVI-noise figures.

Format 4 was used for all low-frequency harmonic data presented.

For broadband noise, format 2 was used. Format 4 was not used because it averages the data on a once per revolution rate, thereby eliminating portions of the broadband noise which are not periodic with the rotor rotation.

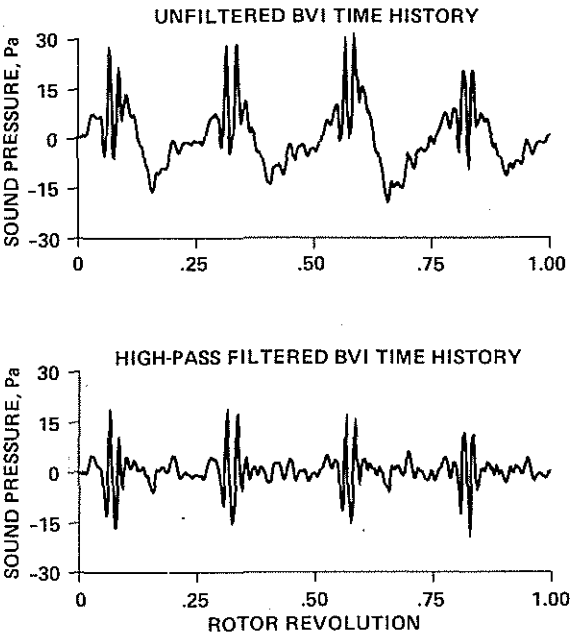

Figure 3. Comparison of unfiltered and high-pass-filtered (220 Hz-10 kHz) BVI time history for microphone 3.

High-Speed Impulsive Noise

High-speed impulsive noise is a combination of linear-thickness and transonic effects.[9] Figure 4 presents peak negative pressure plotted as a function of advancing tip Mach number (M_{AT}) for microphone 1 (the inplane microphone 1.5 diameters directly ahead of the rotor hub). Microphone 1 was chosen for data presentation because HSI noise is known to radiate predominantly inplane.[9] At M_{AT} below 0.80 the rate of change of the sound pressure is small with changing M_{AT}. Above $M_{AT} \approx 0.80$ the data must be separated into various cases based on the value of M_H. The three cases used were case 1) $M_H < 0.636$; case 2) $M_H = 0.636$;

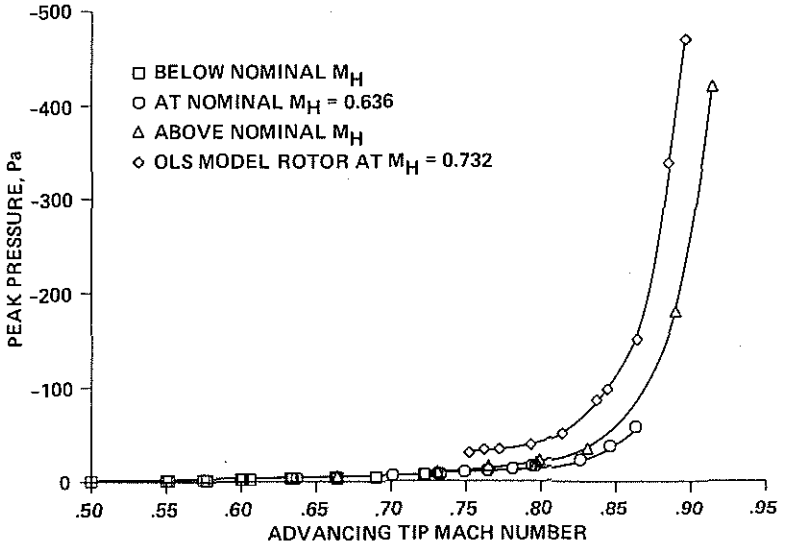

Figure 4. Peak pressure versus M_{AT} for microphone 1.

and case 3) $M_H > 0.636$. The $M_H = 0.636$ value was chosen to differentiate the three cases because that was the designed nominal hover tip Mach number ($M_{H_{NOM}}$). In figure 4 the expected trend of increasing peak negative pressure with increasing M_{AT} is presented with the three different cases represented by different symbols (squares, octagons, and triangles, respectively). At $M_{AT} = 0.80$ the case 2 and case 3 data both begin to diverge, but at different rates. The case 3 sound pressure begins to increase first and more rapidly because the rotor is at a higher velocity all around the rotor disc than in case 2 (except for $\psi = 90°$). This increased M_H produces more noise, hence the separation at $M_{AT} = 0.80$ between case 2 and case 3 data. Case 2 appears to follow the case 3 trend, although the starting point is at a slightly higher M_{AT}.

One additional curve is included in figure 4. This curve (distinguished by the diamond markers) presents the sound pressure of the Operational Loads Survey (OLS) blade tested in the DNW in 1982,[10] allowing a comparison between the sound pressure of an older rotor and a lower tip speed, newer technology rotor.

As M_{AT} increases, the HSI-noise signature exhibits waveform changes. Figure 5 presents one blade-passage time history at three different and increasing advancing tip Mach numbers. As M_{AT} increases, the waveform changes from a symmetric, smooth pulse to an impulsive shape. The symmetric pulse becomes increasingly triangular, and at $M_{AT} = 0.913$ the compression side of the acoustic wave is nearly vertical, indicating that a shocklike wave has propagated to the far field. This shocklike propagation from the rotor blade is called delocalization.[9] For the OLS blade, delocalization occurs at $M_{AT} = 0.89$, a difference in Mach number of approximately 0.02. This increase of delocalization Mach number is most likely due to the reduced chord length and the thinner airfoil of the BH 360.

The HSI-noise data presented in figure 4 are also presented in the frequency domain in figure 6. Figure 6 is a plot of the sound pressure level (SPL) of the fundamental and first 14 harmonics of the case 3 data, as a function of M_{AT}. It shows that the impulsiveness of the signature with increasing M_{AT}, seen in figure 5 in the time domain, corresponds to an energy increase in the higher harmonics. This increase in harmonic energy becomes increasingly important beginning at $M_{AT} = 0.83$, where the first harmonic has more energy

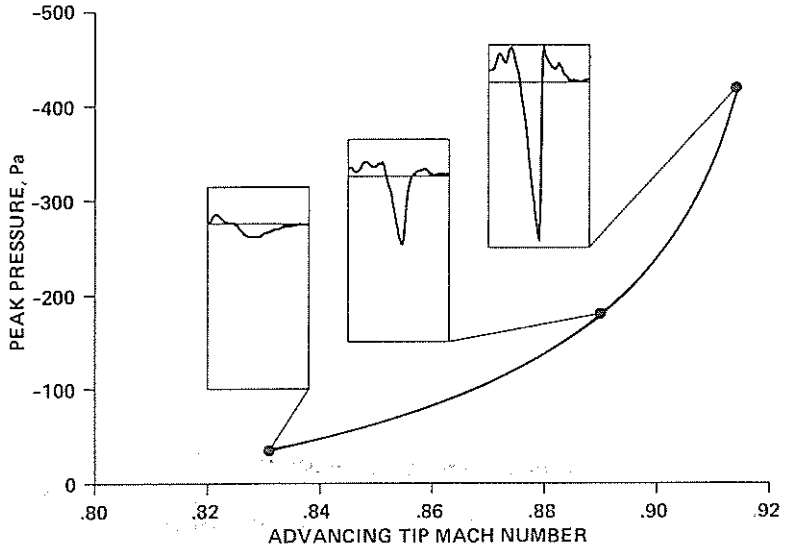

Figure 5. Waveform shape versus M_{AT} for microphone 1.

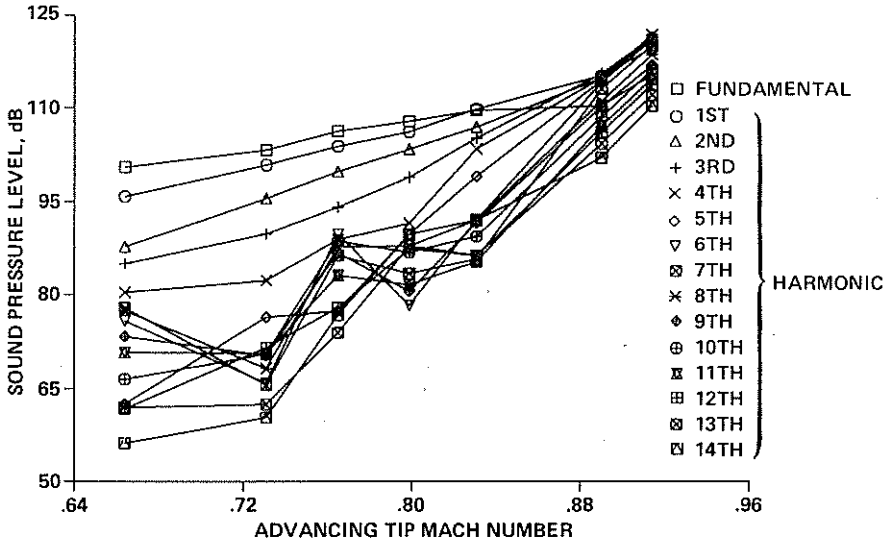

Figure 6. Energy in the first 14 harmonics versus M_{AT} for microphone 1.

than the fundamental. Figure 7 shows that at $M_{AT} = 0.89$ the first 8 harmonics have more energy than the fundamental, and at $M_{AT} = 0.913$ there are 10 harmonics with more energy than the fundamental. This harmonic representation of the HSI noise clearly conveys the importance of incorporating higher harmonics in HSI-noise prediction codes.

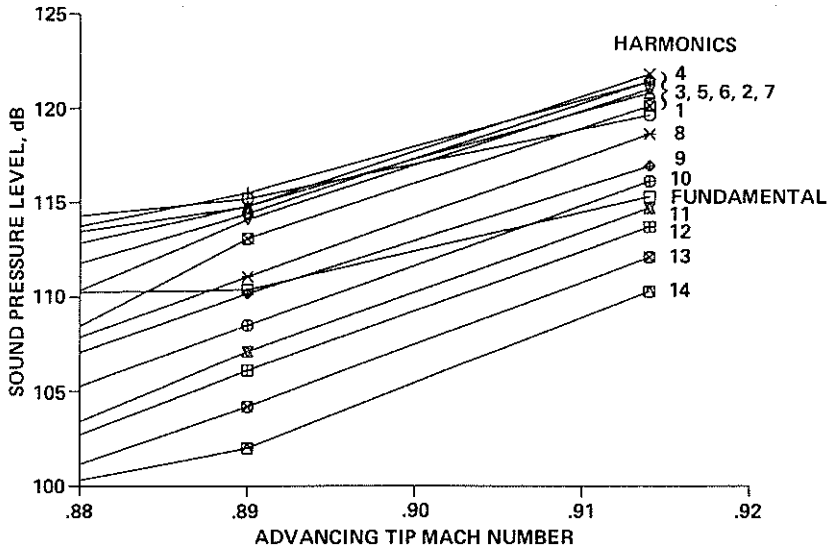

Figure 7. High-speed harmonic energy versus M_{AT} for microphone 1.

Blade-Vortex Interaction Noise

BVI noise is generated when one rotor blade intersects or passes close to a vortex generated by itself or by a previous blade. The noise generation is a function of 1) vortex strength, 2) vortex size, 3) angle of interaction between blade and vortex line, and 4) vertical separation between the blade and the vortex. In terms of helicopter flight parameters, BVI is influenced by advancing tip Mach number, rate of descent, advance ratio, and thrust coefficient.[9]

Changes in BVI noise resulting from variations in the rate of descent and the advance ratio are discussed first. In wind tunnel testing the desired rate of descent can be achieved by tilting the shaft back (positive shaft-tilt angles). Changes in advance ratio were achieved by changing the wind velocity in the tunnel while keeping M_H constant. A matrix of 8 shaft-tilt angles and 7 advance ratios was performed to locate the conditions for maximum BVI noise. One effective format for an overall qualitative and quantitative data presentation is similar to that used by Cox in 1984,[11] now known as the "fried egg" plot. This three-dimensional mapping of shaft-tilt angle (rate of descent) versus advance ratio (forward velocity) versus filtered PTP pressure is presented in a color contour map. Color contouring was used because it clearly shows a large amount of data in a compact format. The colors correspond to the filtered PTP pressures; because the pressures have such a large range in magnitude (1.0 Pa to 50.0 Pa), a logarithmic color scale was used. This scale is shown in figure 8 and will be used for figures 9 through 13. Figure 9 maps shaft-tilt angle versus advance ratio for microphone 9. Microphone 9 is located 3.0 rotor radii away from the rotor hub, 25° below the rotor plane, at an azimuthal angle of 150°. Figure 11 presents the BVI maps for 13 microphones at 3.0 rotor radii (microphones 1-13). All the maps in figure 11 show that at low μ and low α_s (lower left corner) the least amount of BVI noise is generated. At low μ the BVI noise increases with increasing α_s, and at low α_s the BVI noise increases with increasing μ. A line drawn diagonally between the upper left corner and the lower right corner represents the conditions for maximum BVI noise. This is the same trend that was found for the OLS wind tunnel and OLS flight-test data.[4]

A representative directivity map is shown in Figure 10 at one shaft-tilt angle (α_s = 3.0°) and one advance ratio (μ = 0.198). The abscissa is the azimuthal angle and the ordinate is the elevation angle for each of the first 13 microphones. BVI noise is known to have a preferred radiation direction.[9] For a presentation of the directivity associated with BVI noise, directivity maps for microphones 1-13 are shown in figures 12 and 13. Figure 12 presents data for μ = 0.150, and figure 13 for μ = 0.198. On each directivity map the largest interaction noise occurs at least 25° below the plane of the rotor. This was true for both the OLS wind tunnel test data[4] and the OLS flight-test data.[4] Occasionally the noise initially propagates directly ahead of the rotor (figure 12), but the maximum BVI noise always radiates toward the advancing side with increasing shaft-tilt angle.

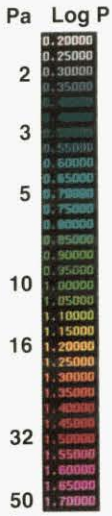

Figure 8. Color scale for filtered, PTP, 64-revolution-averaged, blade to blade averaged, acoustic pressures.

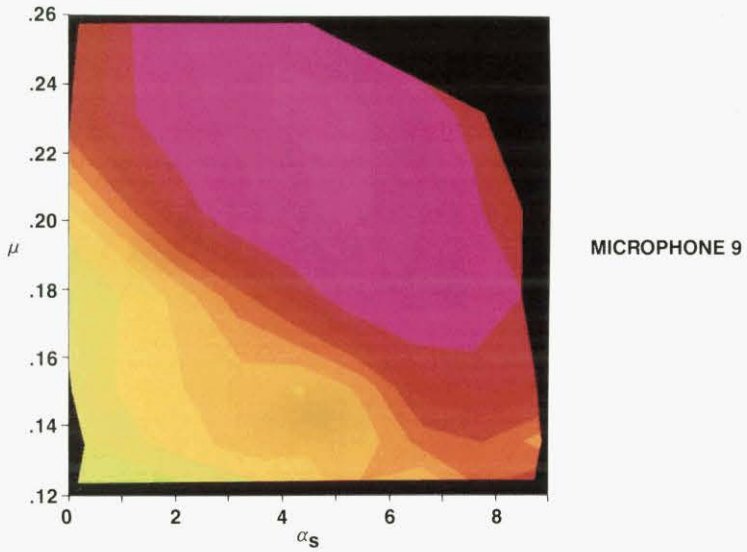

Figure 9. Conditions for maximum BVI noise based on filtered, averaged, PTP acoustic pressure for microphone 9.

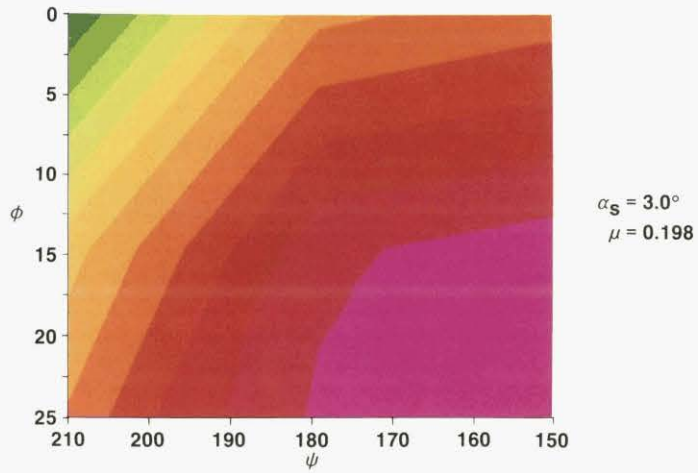

Figure 10. Directivity map for filtered, averaged, PTP acoustic pressure at μ = 0.198 and α_S = 3.0.

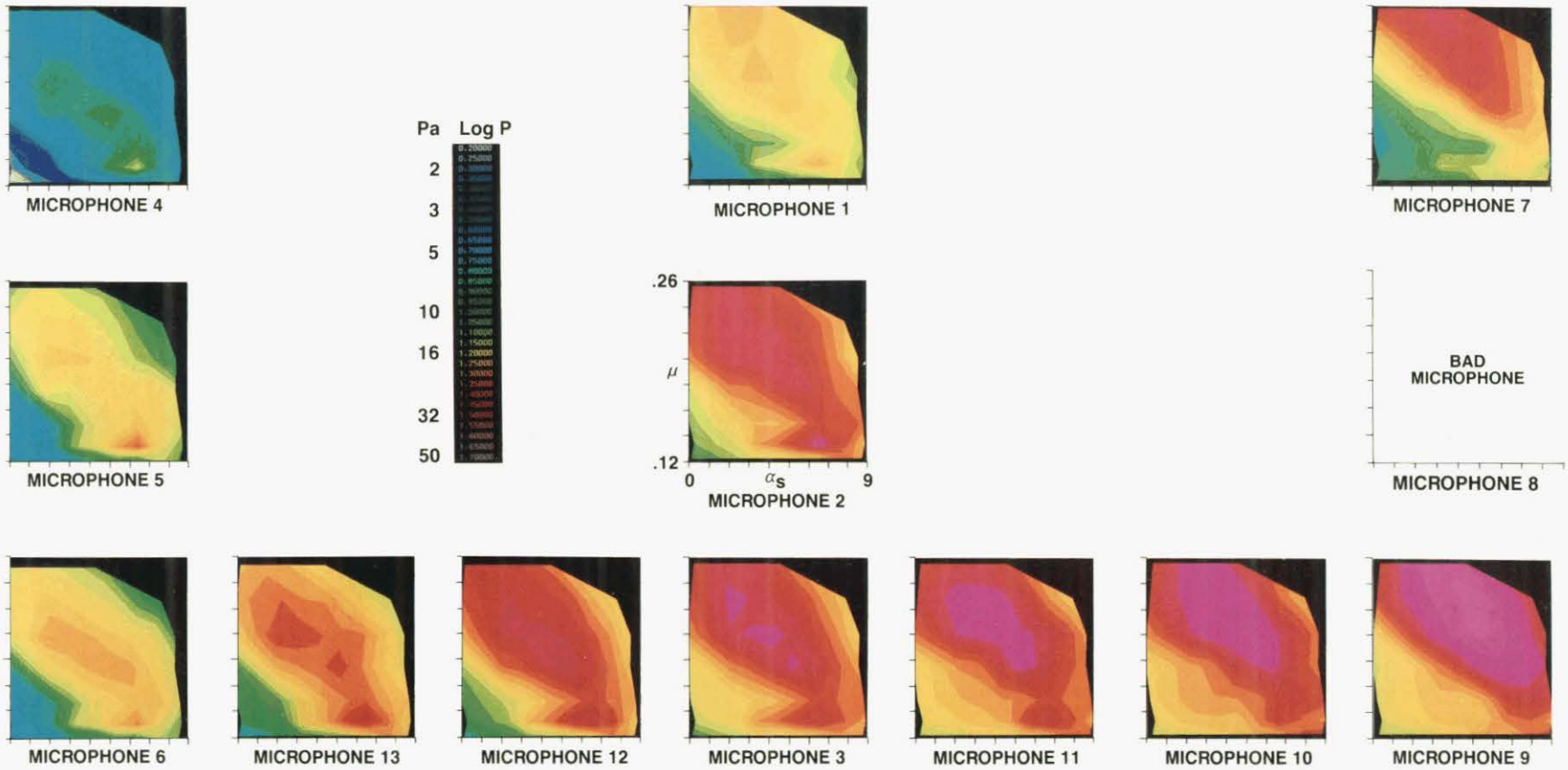

Figure 11. Conditions for maximum BVI noise based on filtered, averaged, PTP acoustic pressure for microphones 1-13.

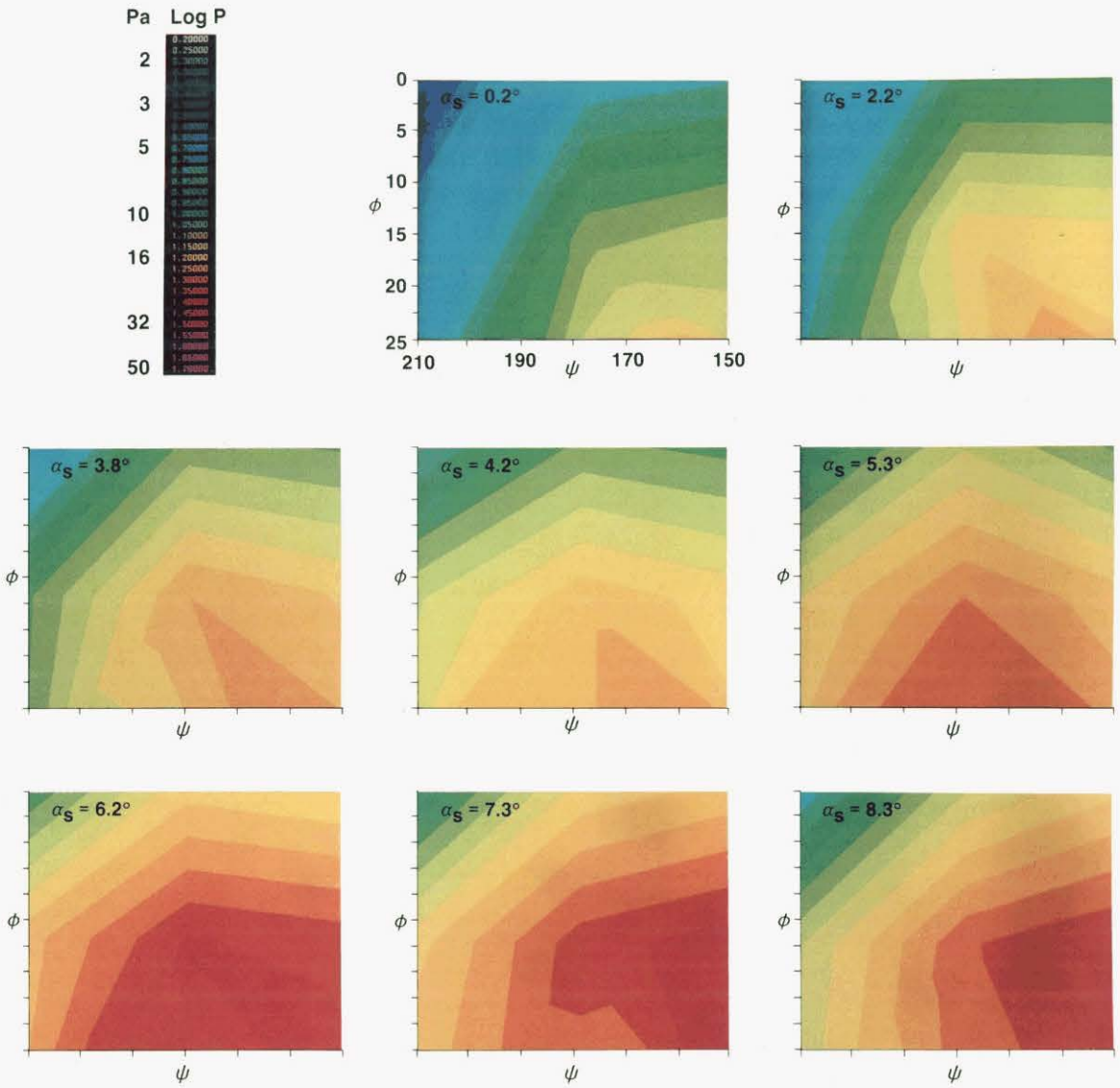

Figure 12. Directivity map, shaft-angle sweep for filtered, averaged, PTP acoustic pressure at $\mu = 0.150$.

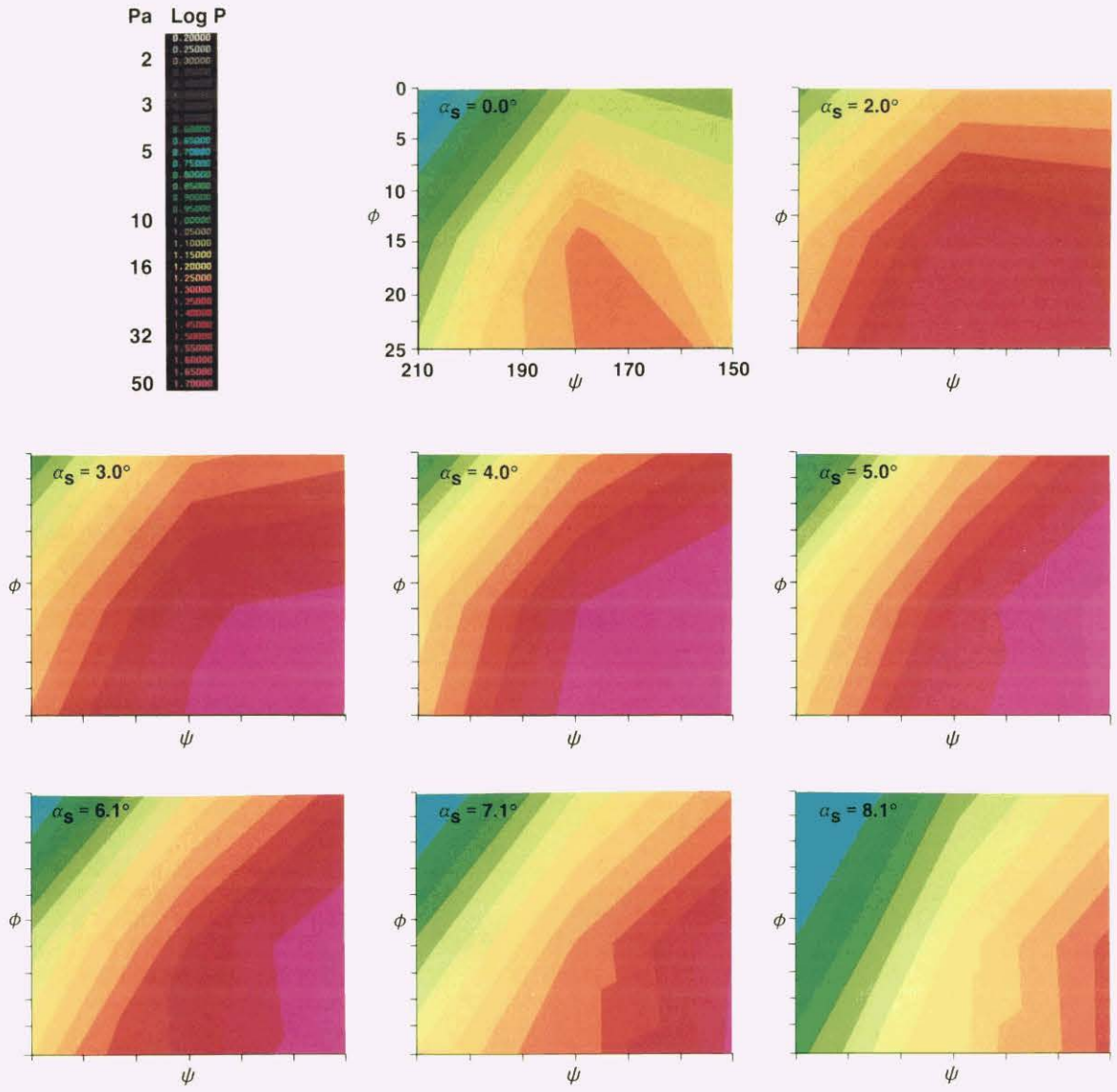

Figure 13. Directivity map, shaft-angle sweep for filtered, averaged, PTP acoustic pressure at $\mu = 0.198$.

The final parameter to be presented which affects BVI noise is thrust. Figures 14 and 15 present the PTP, filtered, BVI-noise time histories at three different thrust values for advance ratios of 0.150 and 0.198, respectively. As the thrust increases, the strength of the vortex increases, resulting in higher noise levels during interactions. The magnitude of this increased pressure is shown in figures 16 and 17 as a function of thrust, at the two advance ratios. Although not linear, a doubling of sound pressure amplitude occurs with a doubling of thrust. This result is similar to that found for the OLS wind tunnel test data.[4]

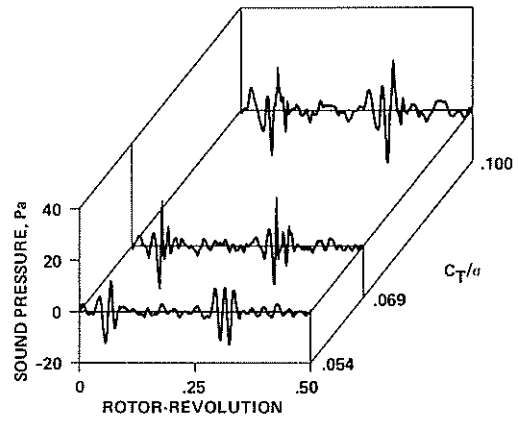

Figure 14. BVI waveform comparisons for microphone 3 at μ=0.150.

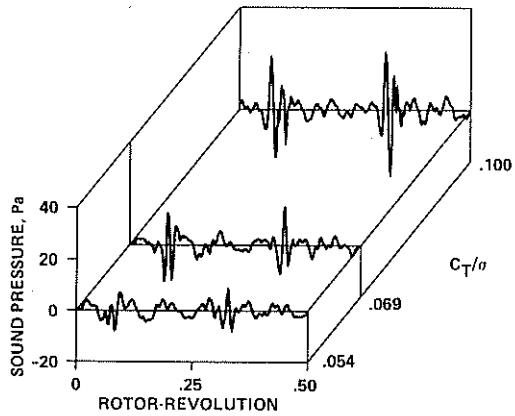

Figure 15. BVI waveform comparisons for microphone 3 at μ=0.198.

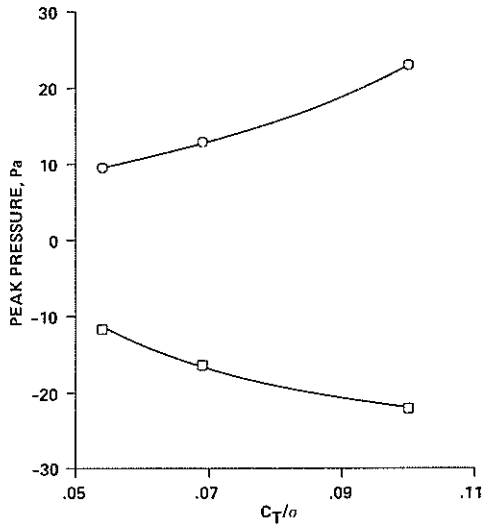

Figure 16. Peak BVI pressures for microphone 3 at μ=0.150.

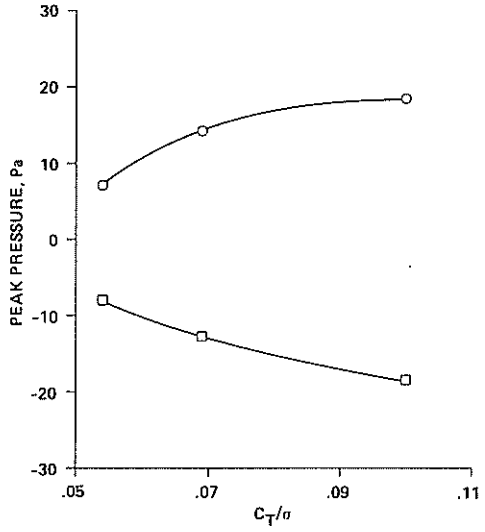

Figure 17. Peak BVI pressures for microphone 3 at μ=0.198.

Low-Frequency Noise

Facilities capable of good quality low-frequency rotor acoustic data acquisition are rare. The DNW is one of the few facilities specifically designed as an aeroacoustic tunnel, and with its large size and low-frequency acoustic treatment it is suitable for low-frequency rotor noise measurements. Since the blade passage frequency (BPF) of the BH 360 is approximately 88 Hz, well below the cutoff frequency of many other tunnels,[12] these test data provide a unique opportunity for low-frequency model-to-full-scale data comparisons.

To apprise the characteristics of the facility, rates of noise decay with distance were examined as a function of harmonic number and Mach number. The inplane microphones used for the low-frequency data in figures 18-21 were 1, 4, and 7 at 1.5 D; 14 at 3.0 D; 21 at 4.6 D; and 25 and 26 at 6.5 D, where D is rotor diameter. Because these microphones were located at different azimuthal angles, only hover data can be used. Theoretically if the rotor is in hover, microphones at equal distances from the noise source at different azimuthal angles should have the same SPL, but in practice the testing facility could have some deficiencies near the lower cutoff frequency.

Figure 18 presents the SPL for the sum of the fundamental and first four harmonics, hereafter referred to as "sum", versus M_{AT} at the four distances (1.5 D, 3.0 D, 4.6 D, 6.5 D). In theory the SPL should decay inversely with distance in the far field.[13] This means the 3.0 D microphone SPL should be 6 dB lower than the SPL at 1.5 D, the microphone SPL at 4.6 D should be 9.7 dB lower than the SPL at 1.5 D, and the microphone SPL at 6.5 D should be 12.7 dB lower than the SPL at 1.5 D. From figure 18 we see the microphone 26 SPL data are approximately 6 dB too low. This result was also noted by Aggarawal, Schmitz, and Boxwell.[14] One probable reason for the reduced amplitude is that the acoustic treatment around microphone 26 consisted of only the flat acoustic panels with a cutoff frequency approximately 3.5 times that of the acoustic wedges. Therefore, microphone 26 data will not be used in the decay slopes presented in figures 19 and 20.

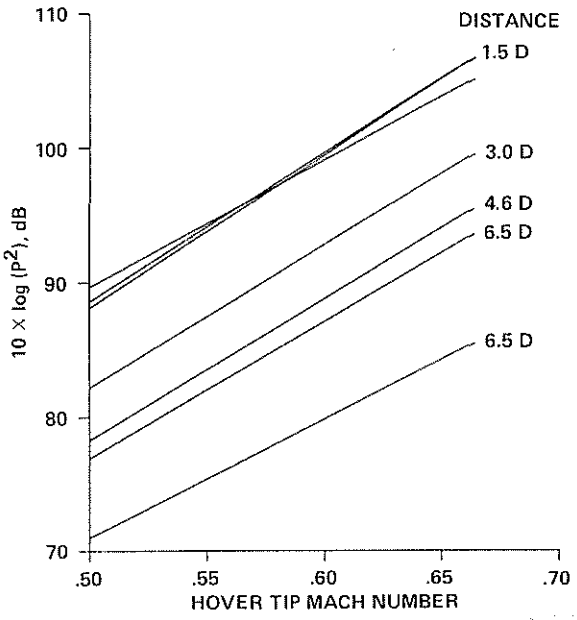

Figure 18. Peak sound pressure levels for the inplane microphones versus M_H.

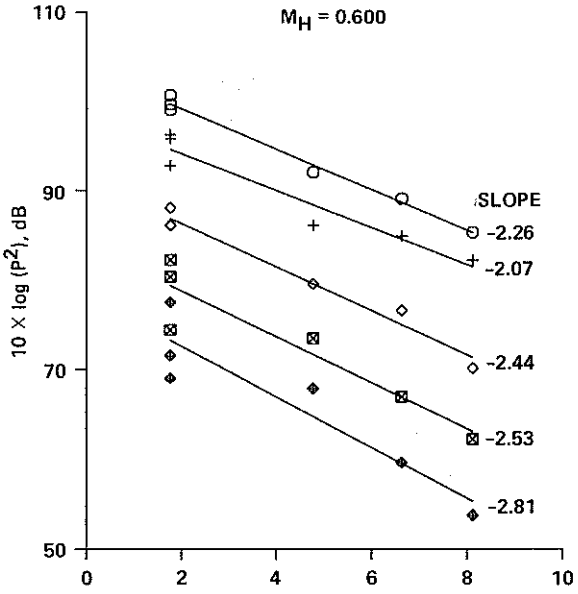

Figure 19. Peak sound pressure levels for the sum, fundamental, and first three harmonics for the inplane microphones versus 10 times the log of the distance, M_H =0.600.

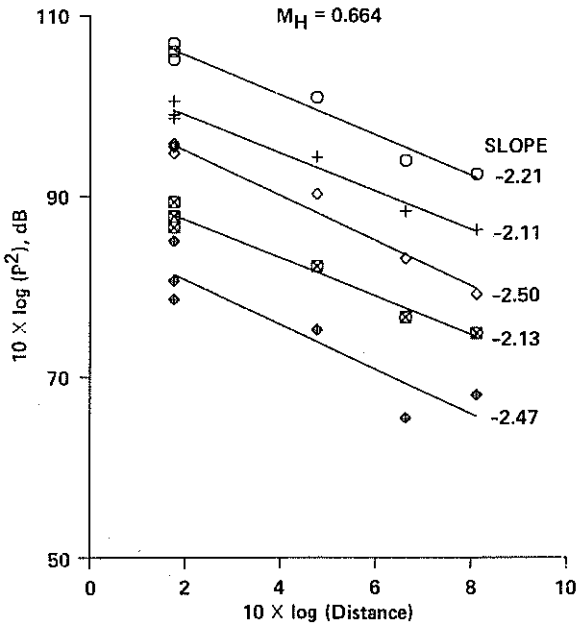

Figure 20. Peak sound pressure levels for the sum, fundamental, and first three harmonics for the inplane microphones versus 10 times the log of the distance, M_H =0.664.

Figures 19 and 20 present the noise decay with distance for the sum, the fundamental, and the first 3 harmonics at $M_H = 0.600$ and $M_H = 0.664$ respectively. The abscissa is 10 times the logarithm of the microphone distance in rotor diameters and the ordinate is 10 times the logarithm of the acoustic pressure squared. With this selection of axes the decay slopes, calculated using a least-squares fit, should theoretically equal -2.0. Although the slopes range from -2.07 to -2.81 these slopes do not depend on either harmonic number or Mach number and therefore good confidence is established for low-frequency data acquisition in this facility.

To observe the effect of M_{AT} on low-frequency noise, figures 21a and 21b present four time histories at four different values of M_{AT} for microphone 1 (located inplane 1.5 D directly ahead of the rotor hub). Changes in M_{AT} were achieved by holding M_H constant at 0.636 and α_s constant at 0°, and increasing the advance ratio. Figure 21b was produced by low-pass-filtering the data in figure 21a from 0 Hz to 300 Hz. At the two higher values of M_{AT} in figure 21a, BVI starts to appear, but it was eliminated by the filtering in 21b. Both figures 21a and 21b show an increase in thickness noise with increasing M_{AT}.

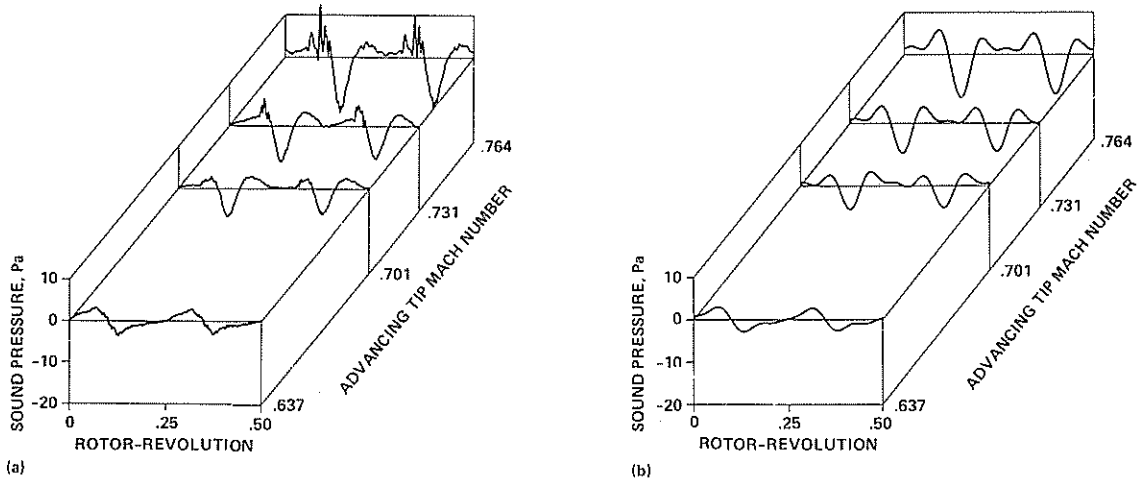

Figure 21. Low-frequency waveform comparison for four advancing tip Mach numbers, M_H=0.636: (a) unfiltered, (b) low-pass filtered (0-300 Hz).

Figures 22a and 22b present the effect of thrust change on low-frequency noise. Five time histories are shown for inplane microphone 1. Figure 22b is a 0- to 300-Hz low-pass-filtered version of figure 22a. Two important changes occur with change in thrust: the amplitude changes (this can be seen more clearly in figure 23), and the waveform changes in character. At the lowest C_T/σ value the negative pressure is larger in amplitude than the positive pressure, and the positive pressure seems to "flatten" out. At the highest C_T/σ value the negative and positive pressures are nearly equal in magnitude and more sinusoidal in shape, although a large amount of high-frequency data is riding on top of the low-frequency noise data. This high-frequency noise is most likely caused by an increased unsteadiness in the inflow. These waveform shape changes, as well as amplitude changes, must be captured in low-frequency prediction codes.

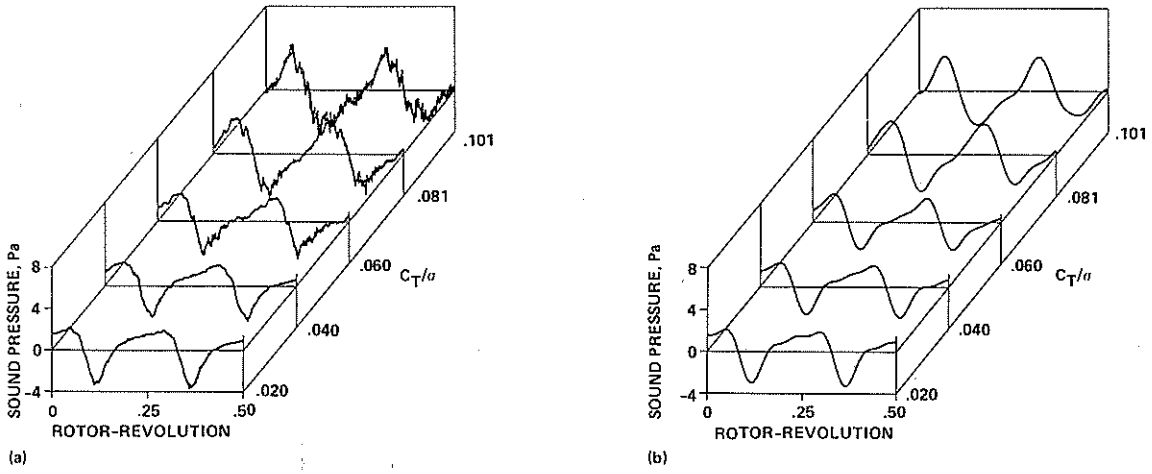

Figure 22. Low-frequency waveform comparison for five thrust values, M_H=0.636: (a) unfiltered, (b) filtered (0-300 Hz).

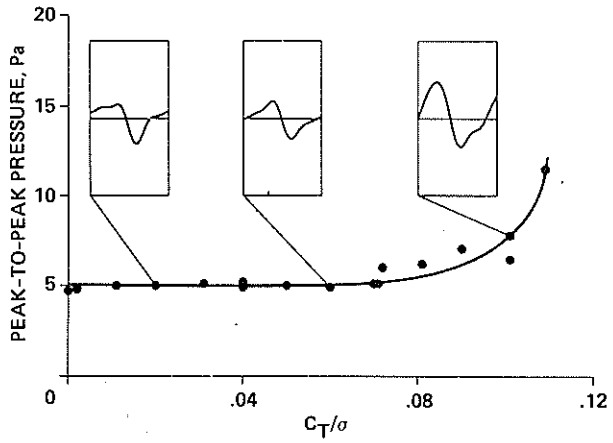

Figure 23. Peak-to-peak sound pressure versus thrust.

Figure 23 presents the filtered peak-to-peak pressure as a function of thrust. Note that the amplitude is not affected by thrust changes below $C_T/\sigma = 0.070$, but starting at $C_T/\sigma = 0.070$ the PTP pressure increases with increasing thrust. One possible explanation for the noise increase is that it is produced by the increase in induced drag resulting from the higher thrust. Also included in figure 23 are filtered blade-passage waveforms at three different thrust levels.

Broadband Noise

Noise can be classified as either discrete (harmonic) or broadband. Broadband rotor noise is a result of unsteady, nondeterministic blade loading.[15]

Broadband noise is often the least considered of the four noise sources because it has, in general, the smallest amplitude. However, research has shown that broadband noise increases in importance relative to discrete noise as rotor speed is reduced. The on-axis

overhead microphone, number 20, was used for all the broadband noise plots. Unfortunately, a flow-visualization technique used for this test required that a 12-ft by 12-ft by 1/2-in.-thick panel also be placed on the ceiling directly over the rotor. The microphone was flush-mounted with the panel surface and centered in a 5-in.-diameter hole. Impulse testing showed that disturbances may result from the presence of the panel. These disturbances, affecting only microphone 20, were present for the entire open-jet test. Their effect is noticeable in figures 24 and 25. The relatively smooth frequency curve normally associated with the on-axis microphone appears to be influenced by the panel to varying levels depending on frequency. Although disturbances do exist, two important trends with thrust change are presented.

In figure 24, four spectra are shown corresponding to four thrust levels. As the thrust is increased from $C_T/\sigma = 0.070$ to $C_T/\sigma = 0.109$, the broadband noise is increased by each thrust change to give a total SPL increase of $\approx$ 15 dB for the entire frequency range. This thrust dependence of BBN is important because the BBN sets the floor for the microphone signal-to-noise ratio.

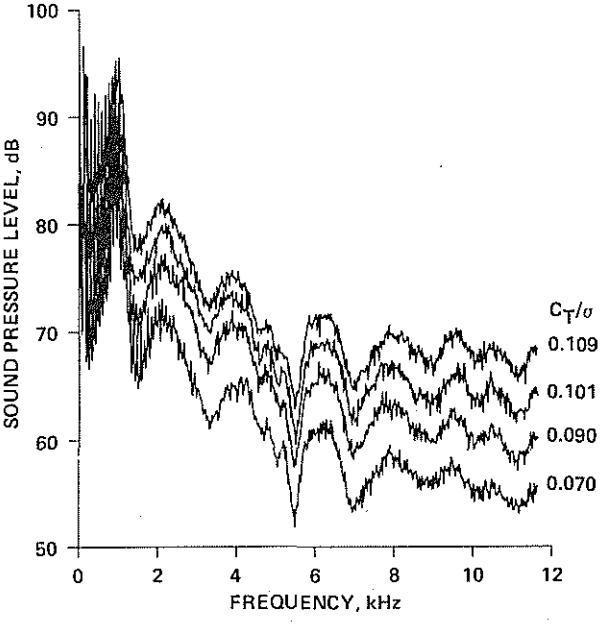

Figure 24. Power spectrum for overhead microphone, number 20, at four thrust values.

In figure 25 two spectra are presented, one corresponding to $C_T/\sigma = 0.002$ and the other to $C_T/\sigma = 0.070$. The lower thrust level is nearly a nonlifting rotor case, so the wake is still in the plane of the rotor. This inplane wake results in a large number of blade-wake interactions (BWI) and accounts for the increased energy at frequencies between 2 and 3.5 kHz for the lower thrusting condition. As the frequency increases, the higher thrusting condition contains more energy, as would be expected.

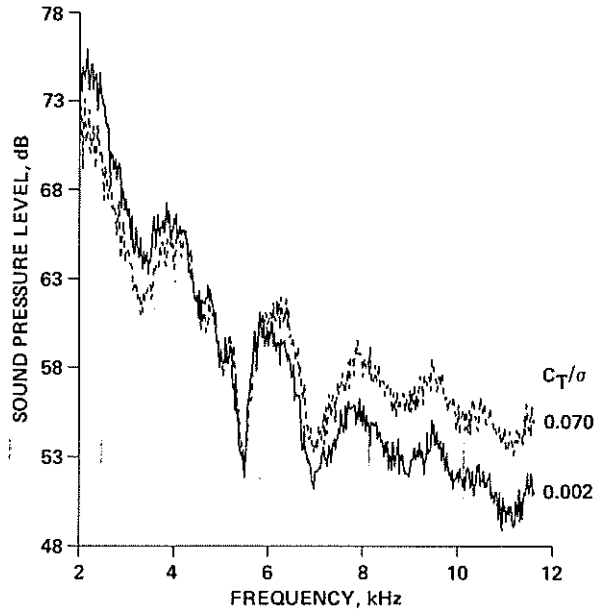

Figure 25. Power spectrum for overhead microphone, number 20, at two thrust values.

4. CONCLUSIONS

High-quality data necessary for acoustic code validation are now available. The expected trends for high-speed impulsive noise, blade-vortex interaction noise, low-frequency noise, and broadband noise have been presented for a 1/5th-scale model of an advanced modern rotor. This data base offers the researcher an opportunity for rotor acoustic insight not only because of the quality of the data but because of the quantity of the data available. Another important asset of this data base is the organization and efficiency with which the data can be accessed and utilized.[3]

A few important trends are summarized. Increasing HSI noise with increasing M_{AT} was shown to result from increased energy in the higher harmonics. BVI noise was found to reach a maximum for conditions ranging from low shaft-tilt angles at high advance ratios to high shaft-tilt angles at low advance ratios. The direction of the maximum radiated BVI noise is at least 25° below the rotor plane and toward the advancing side of the rotor. Because of the large test chamber and extensive acoustic treatment, the DNW is also a suitable testing facility for acquiring the low-frequency portion of the data base. Lastly, anomalies in the data from two microphones, on-axis and inplane at 45° azimuth, were identified.

The objective of this paper was to give the community a first broad look at a comprehensive aeroacoustic rotor data base available today. It is these authors' sincere hope that this data base, in conjunction with the simultaneous pressure data base, will make possible a significant advancement in rotorcraft noise prediction.

5. ACKNOWLEDGMENT

The authors wish to thank all those affiliated with this project. In particular, we would like to thank our many friends and colleagues at the DNW and NLR for their extraordinary efforts in making this experimental program such a success. We would also like to thank Professor Albert George of Cornell University for his fruitful discussions and guidance on broadband noise.

6. REFERENCES

1. H. Hubbard and L. Lassiter, Some Aspects of the Helicopter Noise Problem, *NACA TN 3239*, 1954.
2. H. Sternfeld and E. G. Schaffer, An Investigation of Rotor Harmonic Noise by the Use of Small Scale Wind Tunnel Models, *NASA CR 166337*, 1982.
3. D. A. Boxwell, R. A. Zinner, and H. M. Kodani, Boeing Vertol Model 360 Rotor Acoustic Signature Measurements in the DNW, *AATMR Technical Reports 88-1 through 88-11*, 1988.
4. D. A. Boxwell et al., Helicopter Model Rotor-Blade Vortex Interaction Impulsive Noise: Scalability and Parametric Variations, *J. of Amer. Helicopter Soc.* **32** (1987).
5. F. H. Schmitz et al., A Note on the General Scaling of Helicopter Blade-Vortex Interaction Noise, *AHS 38th Annual Forum*, 1982.
6. J.C.A. van Ditshuizen et al., Acoustic Capabilities of the German-Dutch Wind Tunnel, *AIAA Paper 83-0146*, 1983.
7. J.C.A. van Ditshuizen, Compilation of Calibration Data of the German-Dutch Wind Tunnel, *DNW Report MP-82.01*, 1982.
8. L. Dadone, S. Dawson, and D. Ekquist, Model 360 Rotor Test at DNW - Review of Performance and Blade Airload Data, *AHS 42nd Annual Forum*, 1986.
9. F. H. Schmitz and Y. H. Yu, Helicopter Impulsive Noise: Theoretical and Experimental Status, *J. of Sound Vibration* **109** (1986): 361–422.
10. D. A. Boxwell et al., Model Helicopter Rotor High-Speed Impulsive Noise: Measured Acoustics and Blade Pressures, *NASA TM 85850*, 1983.
11. C. A. Cox, Noise Reduction Potential of Operating Procedures, *Helicopter Noise Reduction Program*, 1984.
12. J. Bender and R. E. A. Arndt, Aeroacoustic Research in Wind Tunnels: A Status Report, *NASA CR 114575*, 1973.
13. L. L. Beranek, Acoustics, *McGraw-Hill Book Company, Inc.*, 1954.
14. H. R. Aggarawal, F. H. Schmitz, and D. A. Boxwell, Prediction and Measurement of Low-Frequency Harmonic Noise of a Hovering Model Helicopter Rotor, *AHS 45th Annual Forum* , 1989.
15. T. F. Brooks et al., Main Rotor Broadband Noise Study in the DNW, *AHS Aerodynamics and Aeroacoustics Specialist's Meeting*, 1987.